IOP Publishing Journal of Physics: Condensed Matter
J. Phys.: Condens. Matter **32** (2020) 165601 (14pp) https://doi.org/10.1088/1361-648X/ab5ce7

Non-equilibrium electronic transport through a quantum dot with strong Coulomb repulsion in the presence of a magnetic field

Denis Zhuravel[1], Dmitry V Anchishkin[1,2], Roland Hayn[3,4], Pierre Lombardo[3,4] and Steffen Schäfer[3,4]

[1] Bogolyubov Institute for Theoretical Physics, Kiev 03143, Ukraine
[2] Taras Shevchenko National University of Kiev, Kiev 03022, Ukraine
[3] Aix-Marseille University, Faculty of Science, St. Jérôme, Marseille, France
[4] Institut Matériaux Microélectronique Nanosciences de Provence, UMR CNRS 7334, Marseilles, France

E-mail: lpbest@ukr.net

Received 26 March 2019, revised 20 November 2019
Accepted for publication 28 November 2019
Published 23 January 2020

Abstract

The non-equilibrium electronic transport through a nanoscale device composed of a single quantum dot between two metallic contacts is studied theoretically within the framework of the Keldysh formalism. The quantum dot consists of a single energy level subject to an applied magnetic field. Correlations due to the Coulomb repulsion between electrons on the dot are treated with a Green's function decoupling scheme which, although similar to the Hubbard-I approximation, captures some of the dynamics beyond. The scheme is exact in the so-called atomic limit, defined by vanishing tunneling between contacts and dot, and in the non-interacting limit, where the on-dot Coulomb repulsion is zero. Explicit analytic solutions, valid for arbitrary magnetic fields, are obtained for two important setups: (i) the stationary regime, with constant voltage bias between the leads, and (ii) the time-dependent regime for metallic leads with constant density of states of infinite width. In these regimes, the current through the dot is evaluated numerically for various parameter sets and its main features interpreted in terms of the underlying physical processes. The results are compared to the non-crossing approximation (NCA) and diagrammatic non-equilibrium quantum Monte-Carlo (QMC) where available.

Keywords: quantum dots, strong electronic correlations, quantum transport, non-equilibrium Green's function techniques

(Some figures may appear in colour only in the online journal)

1. Introduction

In the three decades since the advent of the first gallium arsenide heterostructures with transport signals carrying the signatures of individual electrons, [1–4] the enthusiasm for *quantum dots* (QD), as these nanoscale devices are nowadays labeled, has continuously increased with experimental realizations now including silicon [5, 6] and carbon nanotubes [7]. Such tunable 'artificial atoms' provide an ideal platform to test quantum theory in parameter ranges inaccessible in conventional systems. The studied phenomena range from Coulomb blocking and the quantum Hall effect [8] over Kondo physics, [5, 9] thermoelelectricity [10–14] to non-Fermi liquid behavior, quantum phase transitions and quantum criticality [15–17] Beyond the obvious fundamental interest, the transport properties of QDs are put to use in a host of applications,

including field-effect transistors, [18] photovoltaics [19] and visualization tools for molecular processes in neuroscience [20].

In the present paper, we investigate the electronic transport through a single-orbital QD addressed by two metallic tunneling contacts. Electrons on the otherwise isolated dot experience a strong Coulomb repulsion and, possibly, an applied magnetic field which lifts the spin degeneracy of the orbital via the Zeeman effect. The contacts or leads, by contrast, are modeled as perfect uncorrelated metals not exposed to the magnetic field. The appropriate Hamiltonian for this setup is, of course, the widely studied impurity model introduced by Anderson [21] over 50 years ago to explore the seemingly unrelated topic of localized magnetic moments in transition metals.

Contrary to the systems Anderson aimed to describe with his model, our QD is not in thermal equilibrium but subject to a voltage bias applied between the leads. The transport through the dot has thus to be described by a suitable non-equilibrium formalism, and we opt for Keldysh's version [22–24]. Our theoretical analysis follows the excellent article of Jauho *et al* [25] but, contrary to the latter, accounts for magnetic fields and the on-dot Coulomb repulsion.

The Coulomb repulsion introduces strong electron correlations for which exact solutions are unavailable and approximations inevitable. Among the recent theoretical approaches, we would like to mention Smirnov and Grifoni's [26] Keldysh effective field theory with which they investigated the erosion of the Kondo resonance through an applied magnetic field; the so-called i-DFT employed by Stefanucci and Kurth [27] to explore the crossover from the Kondo to the Coulomb blockade regime; and non-equilibrium Green's functions decoupling schemes like Croy and Saalmann's auxiliary-mode expansion [28], or the slave-boson based SOQRE by Dong *et al* [29].

In parallel, a large variety of numerical approaches have been developed, ranging from numerical renormalization group (NRG), over density matrix renormalization group (DMRG) to quantum Monte Carlo (QMC). These algorithms all give excellent to virtually exact results for equilibrium situations, but run each into their own kind of technical problems—e.g. mixing of high- and low-energy states in RG-based methods, 'dynamical' in addition to the intrinsic fermionic sign problem in QMC—when addressing the dynamics of an out-of-equilibrium system on long time scales, entailing instabilities and an exponential growth of the computational cost (for a discussion, see [30] and references therein). Recently, Cohen *et al*'s [30] 'inchworm' implementation of diagrammatic QMC seems to have eased this problem for evolution times which are not excessively long, and we will test our method against their results.

One of the main drawbacks of purely numerical methods lies in the fact that they give little to no hints to underlying physical processes which might be chiefly responsible for the observed features. Also, the literature advocating for such methods tends to focus on technical aspects like convergence of the numerical scheme at hand, while keeping the experimental layout to a minimum, e.g. pure relaxation after an infinite pulse or switch off [30, 31]. In our opinion, it remains somewhat unclear to what extent such methods are capable of treating more challenging experimental setups.

In this paper, we focus on non-equilibrium transport in presence of a magnetic field and temperature. In this regime, no Kondo physics occurs since the collective screening of the spin on the dot by the contact electrons is known to survive only temperatures, bias voltages and magnetic fields of the order of the Kondo scale [7]. An estimate of the latter is given by Haldane's expression [32, 33],

$$E_K \simeq \sqrt{\Gamma U}\exp\left[-\frac{\pi|\varepsilon_0||\varepsilon_0+U|}{2\Gamma U}\right], \qquad (1)$$

where ε_0 is the dot level measured relative to the zero-bias Fermi level of the leads. Its evaluation shows that the Kondo energy is several orders of magnitude below the temperature and voltage biases we intend to apply, even in absence of a magnetic field.

For the parameter ranges we intend to study, spin fluctuations on the dot are thus suppressed, while charge fluctuations remain important: with the right lead alone, the dot would be driven to an equilibrium configuration in the *empty orbital regime*; however, the voltage bias applied to the left lead ensures that either ε_0 or $\varepsilon_0 + U$ can be addressed such that the dot passes through the *mixed valence regime* [33]. We therefore choose to implement a Green's function decoupling scheme inspired by the so-called Hubbard-I approximation [34, 35] but slightly superior in the rendition of the dynamics. This scheme has already been used by some of the authors [36] in absence of magnetic fields, where it was found to perform comparably to the non-crossing approximation (NCA) [37, 38].

Our extended Hubbard-I decoupling scheme has the following virtues: (i) it is valid for any value of the magnetic field; (ii) it becomes exact in the limits of vanishing Coulomb repulsion and of vanishing lead-dot tunneling; (iii) for the important cases of a stationary voltage bias or with a time-dependent bias but a constant and infinitely wide contact density of states, our method leads to an explicit closed expression for the electric current through the dot, and no iteration procedure is needed; (iv) all Green's function contributions can be represented pictorially, thus suggesting interpretations of the observed spectral features in terms of physical processes; (v) it correctly renders the asymmetry in spectral weight of the two Hubbard bands; [39, 40] (vi) the method produces a perfectly stable long-time dynamics which many numerical methods have great difficulties to capture correctly; [30] and (vii) it is fairly easy to implement, computationally economical and may be adapted to a large variety of experimentally interesting setups.

In this article, we focus on the interplay between Coulomb-induced correlations and magnetic fields, and therefore deliberately neglect phonons, keeping in mind that their contribution to the spectra would have to be incorporated before comparing to the experiment. Typical electron-phonon signatures are side bands and broadened resonances in the

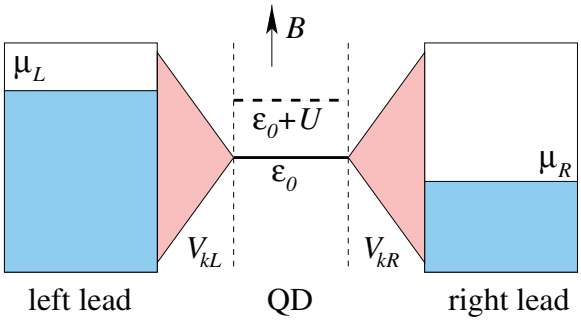

Figure 1. Quantum dot (QD) with a single energy level ε_0, coupled to two metallic leads. Coulomb repulsion U and magnetic field $\mathbf{B}$ are restricted to the dot. Time dependence resides in the dot level ε_0, in the lead levels $\varepsilon_{k\alpha}$, and in the tunneling matrix elements $V_{k\alpha}$.

transport spectra, albeit without affecting the overall tunneling properties between leads and dot [25, 41].

The paper is outlined as follows: section 2 contains a schematic sketch of the experimental setup and its description in terms of Anderson's impurity model; in section 3, we establish the exact equation-of-motion hierarchy for the impurity Green's function and decouple it by means of the aforementioned extended Hubbard-I approximation; in sections 4 and 5, the decoupled Green's function equations are explicitly solved for the current through the dot in the cases of, respectively, a stationary voltage and magnetic bias, and rectangular pulsed biases applied to a dot with wide-band contacts; section 6 contains the numerical results along with benchmarks against state-of-the-art numerical methods and their interpretation in physical terms, and section 7 the conclusions. Details of the numerical method are deferred to appendix.

2. Model Hamiltonian

In the present paper, we study a central quantum dot coupled to two metallic leads as schematically illustrated in figure 1. The Hamiltonian of the electronic system is the sum of three contributions,

$$H = H_{\text{leads}} + H_{\text{tun}} + H_{\text{dot}}, \tag{2}$$

the first of which describes the two metallic leads,

$$H_{\text{leads}} = \sum_{k\alpha\sigma} \varepsilon_{k\alpha}(t)\, \mathbf{c}^{+}_{k\alpha\sigma}\mathbf{c}_{k\alpha\sigma}\,, \tag{3}$$

where $\varepsilon_{k\alpha}(t)$ represents the time-dependent energy levels in the left ($\alpha = L$) and right ($\alpha = R$) lead. $\mathbf{c}^{+}_{k\alpha\sigma}$ and $\mathbf{c}_{k\alpha\sigma}$ are second-quantized creation and annihilation operators for electrons of spin $\sigma \in \{\uparrow,\downarrow\} \equiv \{+,-\}$ with respect to a quantization direction given by the magnetic field in the dot region. Note that both, Coulomb repulsion and magnetic field, are absent on the leads.

The second contribution,

$$H_{\text{tun}} = \sum_{k\alpha\sigma} \left[V_{k\alpha}(t)\, \mathbf{c}^{+}_{k\alpha\sigma}\mathbf{d}_{\sigma} + V^{*}_{k\alpha}(t)\, \mathbf{d}^{+}_{\sigma}\mathbf{c}_{k\alpha\sigma}\right]\,, \tag{4}$$

describes the tunneling between the leads and the dot, with $\mathbf{d}^{\pm}_{\sigma}$ electronic creation and annihilation operators on the dot. The last contribution describes the central dot,

$$H_{\text{dot}} = \varepsilon_0(t) \sum_{\sigma} \mathbf{n}_{\sigma} + \mu_B B(t)\,[\mathbf{n}_{\uparrow} - \mathbf{n}_{\downarrow}] + U\,\mathbf{n}_{\uparrow}\mathbf{n}_{\downarrow}\,, \tag{5}$$

where $\mathbf{n}_{\sigma} = \mathbf{d}^{+}_{\sigma}\mathbf{d}_{\sigma}$ are electron number operators. The first two terms represent a single time-dependent energy level $\varepsilon_0(t)$, split by a Zeeman term, with $B(t)$ an also time-dependent magnetic field and $\mu = \mu_B\,[\mathbf{n}_{\uparrow} - \mathbf{n}_{\downarrow}]$ the magnetic moment residing on the dot. μ_B is the Bohr magneton including the Landé factor. The last term describes the Coulomb repulsion $U(>0)$ between electrons on the dot. We are interested in cases where the Coulomb repulsion is comparable or even exceeds ε_0—a parameter range clearly beyond the scope of perturbation theory.

Time dependence enters in three independent ways: (i) via the energy level $\varepsilon_0(t)$ of the quantum dot and/or the magnetic field $B(t)$; (ii) by a time-dependent overall shift of all energy levels in each lead, $\varepsilon_{k\alpha}(t) = \varepsilon^0_k + \Delta_{\alpha}(t)$; and (iii) via time-dependent tunneling matrix elements which are assumed to be the product of a global time-dependent function times the matrix elements of the time-independent case, i.e. $V_{k\alpha}(t) = u_{\alpha}(t)V^0_{k\alpha}$. Moreover, as in [25], we assume that the tunneling matrix elements depend on k only through the energies ε_k, i.e. $V^0_{k\alpha} = V(\varepsilon^0_{k\alpha})$. This assumption allows for further simplifications.

Experimentally, the described behavior can be implemented by applying time-dependent bias and gate voltages, and by exposing the dot to a time-dependent magnetic field.

3. Electronic transport through the quantum dot

This section is devoted to the description of the time-dependent electronic transport through the dot based on Keldysh's formalism [22] and the corresponding non-equilibrium Green's functions.

In the following, we use notations and general results from the aforementioned article by Jauho *et al* [25] describing the transport through a QD without Coulomb interaction. The current flowing from the left lead to the dot is related to the decrease rate of electrons on the left lead [25]

$$J_L(t) = -e\left\langle \frac{\mathrm{d}}{\mathrm{d}t}N_L(t)\right\rangle = \mathrm{i}\frac{e}{\hbar}\left\langle [N_L, H]\right\rangle\,, \tag{6}$$

where $N_L = \sum_k \mathbf{c}^{+}_{kL}\mathbf{c}_{kL}$ is the total number of electrons on the left lead. Note that the averaging encompasses quantum and thermal expectation values. In the second step of the above equation, the equation of motion for Heisenberg operators

$$\mathrm{i}\hbar\frac{\partial \mathbf{A}(t)}{\partial t} = [\mathbf{A}(t), H(t)] \tag{7}$$

was used. In [25] it was shown that the averages in equation (6) can be expressed through the non-equilibrium Green's functions on the dot, viz.

$$J_L(t) = -2\frac{e}{\hbar}\int_{-\infty}^{t}\mathrm{d}t_1 \int \frac{\mathrm{d}\varepsilon}{2\pi}\mathrm{Im}\sum_{\sigma}\Big\{\mathrm{e}^{-\mathrm{i}\varepsilon(t_1-t)} \times\Gamma^{L}(\varepsilon,t_1,t)\left[G^{<}_{\sigma\sigma}(t,t_1) + f_L(\varepsilon)G^{r}_{\sigma\sigma}(t,t_1)\right]\Big\}\,, \tag{8}$$

where $f_L(\varepsilon)$ is the Fermi distribution and $\Gamma^L(\varepsilon, t_1, t)$ the barrier width of the left lead,

$$\Gamma^{\alpha}(\varepsilon, t_1, t) = 2\pi\rho(\varepsilon)u_{\alpha}(t)u_{\alpha}(t_1)V_{\alpha}(\varepsilon_{\alpha}(t))V^{*}_{\alpha}(\varepsilon_{\alpha}(t_1)) \times \exp\left[\mathrm{i}\int_{t_1}^{t} \mathrm{d}t_2 \Delta_{\alpha}(t_2)\right], \quad (9)$$

for $\alpha \in \{L, R\}$. $\Delta_{\alpha}(t)$ is the time-dependent shift of the lead levels, and $\rho(\varepsilon)$ the density of states per spin in one lead. The latter is assumed to be the same for both leads $\alpha = L, R$.

Finally, equation (8) also makes use of the lesser correlation function and the retarded Green's function on the dot, defined respectively by

$$G^{<}_{\sigma\sigma}(t, t') \;=\; +\frac{\mathrm{i}}{\hbar}\left\langle \mathbf{d}^{+}_{\sigma}(t')\,\mathbf{d}_{\sigma}(t)\right\rangle \quad (10)$$

and

$$G^{r}_{\sigma\sigma}(t, t') = -\frac{\mathrm{i}}{\hbar}\theta(t-t')\left\langle \left\{\mathbf{d}_{\sigma}(t), \mathbf{d}^{+}_{\sigma}(t')\right\}\right\rangle = \square\!\!-\!\!\bullet\,, \quad (11)$$

where the curly brackets stand for anti-commutators, as appropriate for fermionic Green's functions. In the pictorial representation of the last line, the box symbolizes the leads and the horizontal line the dot level which is occupied by one σ-electron shown as a full blue circle. In the following, we adopt units such that $\hbar = k_{\mathrm{B}} = 1$.

3.1. Decoupling scheme for the retarded Green's function

Here, we apply the equation-of-motion technique to the retarded one-electron dot Green's function defined in equation (11). This method yields a closed system of equations and hence the exact Green's function for a QD without interactions. However, in presence of a non-zero Coulomb term on the dot, $U\mathbf{n}_{\uparrow}\mathbf{n}_{\downarrow}$, the equation-of-motion technique generates an endless hierarchy of Green's functions. It is therefore necessary to artificially truncate this hierarchy in order to obtain a closed system of equations. Here, we opt for a decoupling scheme similar to the Hubbard-I approximation: in the first step of our approximation, only σ-electrons (or holes) are allowed to tunnel, while $V_{k\alpha} = 0$ for the opposite spin species, $\bar{\sigma}$; thereafter, the symmetry between both electron species is restored by switching the roles of σ and $\bar{\sigma}$. Our approximations is thus exact for $U = 0$ and in the limit without tunneling, $V_{k\alpha} = 0$, also known as the atomic limit.

In addition to the dot Green's function, introduced in equation (11), our scheme makes use of three higher Green's functions, the first describing the σ-electron after tunneling to the leads, the second and third a $\bar{\sigma}$-fluctuation on the dot plus, respectively, a σ-electron on the dot or on the leads:

$$G^{r}_{k\alpha\sigma\sigma}(t, t') = -\mathrm{i}\theta(t-t')\left\langle \left\{\mathbf{c}_{k\alpha\sigma}(t), \mathbf{d}^{+}_{\sigma}(t')\right\}\right\rangle = \boxed{\bullet}\!\!-\!\!\circ\,, \quad (12)$$

$$G^{r}_{\sigma\sigma,U}(t, t') = -\mathrm{i}\theta(t-t')\left\langle \left\{\mathbf{d}_{\sigma}(t)\mathbf{d}^{+}_{\bar{\sigma}}(t)\,\mathbf{d}_{\bar{\sigma}}(t), \mathbf{d}^{+}_{\sigma}(t')\right\}\right\rangle = \square\!\!\begin{array}{l}\bullet\bullet\\ -\!\!\circ\end{array}\,, \text{ and} \quad (13)$$

$$G^{r}_{k\alpha\sigma\sigma,U}(t, t') = -\mathrm{i}\theta(t-t')\left\langle \left\{\mathbf{c}_{k\alpha\sigma}(t)\mathbf{d}^{+}_{\bar{\sigma}}(t)\,\mathbf{d}_{\bar{\sigma}}(t), \mathbf{d}^{+}_{\sigma}(t')\right\}\right\rangle = \boxed{\bullet}\!\!\begin{array}{l}\bullet\circ\\ -\!\!\circ\end{array}\,. \quad (14)$$

Again, in the graphs, both leads are depicted as a single box, the dot by the horizontal line, electrons and holes by full and empty circles, and spin σ and $\bar{\sigma}$ by the colors blue and red, appearing as black and gray without color, respectively. In the following, all equations of motion are taken from the l.h.s., i.e. with respect to time t. Thus the r.h.s. of the Green's functions, containing operators at time t', never changes and we omit it from the pictograms.

We start from the equation of motion for the dot Green's function (11),

$$\left[\mathrm{i}\frac{\partial}{\partial t} - \varepsilon_0(t) - \mu_B B\sigma\right] G^{r}_{\sigma\sigma}(t, t') = \delta(t-t') + \sum_{k\alpha} V^{*}_{k\alpha}(t) G^{r}_{k\alpha\sigma\sigma}(t, t') + U\, G^{r}_{\sigma\sigma,U}(t, t'), \quad (15a)$$

or, pictorially,

$$\square\!\!-\!\!\bullet \;\Rightarrow\; V \times \boxed{\bullet}\!\!-\!\!\circ + U \times \square\!\!\begin{array}{l}\bullet\bullet\\ -\!\!\circ\end{array}. \quad (15b)$$

Applying the same procedure to the first of the higher Green's functions, $G^{r}_{k\alpha\sigma\sigma}(t, t')$, brings us back to the original dot Green's function:

$$\left[\mathrm{i}\frac{\partial}{\partial t} - \varepsilon_{k\alpha}(t)\right] G^{r}_{k\alpha\sigma\sigma}(t, t') = V_{k\alpha}(t)\, G^{r}_{\sigma\sigma}(t, t') \quad (16a)$$

$$\boxed{\bullet}\!\!-\!\!\circ \;\Rightarrow V \times \square\!\!-\!\!\bullet\,. \quad (16b)$$

The dynamics of the second higher Green function, $G^{r}_{\sigma\sigma,U}(t, t')$, is more complicated since electrons and holes of both spin species may tunnel to the dot, i.e.

$$\begin{aligned}&\left[\mathrm{i}\frac{\partial}{\partial t} - \varepsilon_0(t) - U - \mu_B B\sigma\right] G^{r}_{\sigma\sigma,U}(t, t')\\ &= \delta(t-t')\, n_{\bar{\sigma}}(t) + \sum_{k\alpha} V^{*}_{k\alpha}(t) G^{r}_{k\alpha\sigma\sigma,U}(t, t')\\ &- \mathrm{i}\theta(t-t')\sum_{k\alpha} V_{k\alpha}(t)\left\langle \left\{\mathbf{c}^{+}_{k\alpha\bar{\sigma}}(t)\mathbf{d}_{\sigma}(t)\mathbf{d}_{\bar{\sigma}}(t), \mathbf{d}^{+}_{\sigma}(t')\right\}\right\rangle\\ &- \mathrm{i}\theta(t-t')\sum_{k\alpha} V^{*}_{k\alpha}(t)\left\langle \left\{\mathbf{c}_{k\alpha\bar{\sigma}}(t)\mathbf{d}_{\sigma}(t)\mathbf{d}^{+}_{\bar{\sigma}}(t), \mathbf{d}^{+}_{\sigma}(t')\right\}\right\rangle, \end{aligned} \quad (17a)$$

with $n_{\bar{\sigma}}(t) \equiv \langle \mathbf{n}_{\bar{\sigma}}(t)\rangle$ from now onward. Pictorially, this translates to

$$\square\!\!\begin{array}{l}\bullet\bullet\\ -\!\!\circ\end{array} \;\Rightarrow\; V\times\boxed{\bullet}\!\!\begin{array}{l}\bullet\circ\\ -\!\!\circ\end{array} + V\times\boxed{\circ}\!\!\begin{array}{l}\bullet\bullet\\ -\!\!\circ\end{array} + V\times\boxed{\bullet}\!\!\begin{array}{l}\bullet\circ\\ -\!\!\circ\end{array}. \quad (17b)$$

In order to obtain a closed system of equations, the last two Green functions introduced in the latter equation will be neglected. Physically, this approximation can be motivated as follows: (i) for the large U we are interested in, the system will tend to avoid double occupancies on the dot, and therefore suppress probability amplitudes containing $\mathbf{d}_{\sigma}\mathbf{d}_{\bar{\sigma}}$ as present in the second Green's functions on the r.h.s. of (17); and (ii) a sufficiently large magnetic field fixes a preferred spin direction and therefore suppresses spin-flip contributions involving $\mathbf{d}_{\sigma}\mathbf{d}^{+}_{\bar{\sigma}}$ which makes the last Green's

function on the r.h.s. of (17) negligible. Therefore, we will retain only the dominant first Green's function in (17), $G^r_{k\alpha\sigma\sigma,U}(t,t') = -\mathrm{i}\theta(t-t')\left\langle\left\{\mathbf{c}_{k\alpha\sigma}(t)\mathbf{d}^+_{\bar\sigma}(t)\mathbf{d}_{\bar\sigma}(t),\mathbf{d}^+_\sigma(t')\right\}\right\rangle$, which describes an ordinary σ-electron dynamics, albeit in presence of a $\bar\sigma$-fluctuation on the dot.

In the conventional Hubbard-I decoupling, [35] one would now factorize $\left\langle\left\{\mathbf{c}_{k\alpha\sigma}(t)\mathbf{d}^+_{\bar\sigma}(t)\mathbf{d}_{\bar\sigma}(t),\mathbf{d}^+_\sigma(t')\right\}\right\rangle \simeq n_{\bar\sigma}(t)\left\langle\{\mathbf{c}_{k\alpha\sigma}(t),\mathbf{d}^+_\sigma(t')\}\right\rangle$. In this paper, however, we opt for a more accurate decoupling scheme that—although similar to Hubbard-I—accounts for some of the dynamics neglected by the latter. We establish one more equation of motion:

$$\begin{aligned}\left[\mathrm{i}\frac{\partial}{\partial t}-\varepsilon_{k\alpha}(t)\right]G^r_{k\alpha\sigma\sigma,U}(t,t') &= V_{k\alpha}(t)\,G^r_{\sigma\sigma,U}\\ &+\mathrm{i}\theta(t-t')\sum_{k'\alpha'}V_{k'\alpha'}(t)\left\langle\left\{\mathbf{c}_{k\alpha\sigma}(t)\mathbf{c}^+_{k'\alpha'\bar\sigma}(t)\mathbf{d}_{\bar\sigma}(t),\mathbf{d}^+_\sigma(t')\right\}\right\rangle\\ &-\mathrm{i}\theta(t-t')\sum_{k'\alpha'}V^*_{k'\alpha'}(t)\left\langle\left\{\mathbf{c}_{k\alpha\sigma}(t)\mathbf{d}^+_{\bar\sigma}(t)\mathbf{c}_{k'\alpha'\bar\sigma}(t),\mathbf{d}^+_\sigma(t')\right\}\right\rangle\end{aligned} \tag{18a}$$

or

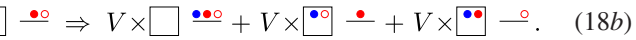

(18b)

In the same spirit as before and similar to what was used by Anderson, [21] we retain only the dynamics of the (blue) σ-electron, which amounts to neglecting the second and the third contribution on the r.h.s.. With these approximations the system of differential equations (15)–(18) is now closed.

We introduce the zero tunneling or, equivalently, atomic limit Green's functions for the dot and each lead,

$$g^r_{0(U),B}(t,t') = -\mathrm{i}\theta(t-t')\,\exp\left[-\mathrm{i}\int_{t'}^t \mathrm{d}t_1\varepsilon_{0(U)}(t_1)-\mathrm{i}\int_{t'}^t \mathrm{d}t_1\mu_B B\sigma\right] \tag{19}$$

$$g^r_{k\alpha}(t,t') = -\mathrm{i}\theta(t-t')\,\exp\left[-\mathrm{i}\int_{t'}^t \mathrm{d}t_1\varepsilon_{k\alpha}(t_1)\right]\,, \tag{20}$$

where henceforth the shorthand $\varepsilon_U \equiv \varepsilon_0 + U$ will be used for the excitation energy to and from the doubly-occupied dot. The equations of motions can now be converted to the following closed system of integral equations:

$$\begin{aligned}G^r_{\sigma\sigma}(t,t') &= g^r_{0,B}(t,t')\\ &+\int_{t'}^t \mathrm{d}t_1\,g^r_{0,B}(t,t_1)\left[\sum_{k\alpha}V^*_{k\alpha}(t_1)G^r_{k\alpha\sigma\sigma}(t_1,t')+U\,G^r_{\sigma\sigma,U}(t_1,t')\right]\end{aligned} \tag{21}$$

$$G^r_{k\alpha\sigma\sigma}(t,t') = \int_{t'}^t \mathrm{d}t_1\,g^r_{k\alpha}(t,t_1)\,V_{k\alpha}(t_1)\,G^r_{\sigma\sigma}(t_1,t') \tag{22}$$

$$\begin{aligned}G^r_{\sigma\sigma,U}(t,t') &= g^r_{U,B}(t,t')\,n_{\bar\sigma}(t')\\ &+\int_{t'}^t \mathrm{d}t_1 g^r_{U,B}(t,t_1)\sum_{k\alpha}V^*_{k\alpha}(t_1)\,G^r_{k\alpha\sigma\sigma,U}(t_1,t')\end{aligned} \tag{23}$$

$$G^r_{k\alpha\sigma\sigma,U}(t,t') = \int_{t'}^t \mathrm{d}t_1\,g^r_{k\alpha}(t,t_1)\,V_{k\alpha}(t_1)\,G^r_{\sigma\sigma,U}(t_1,t'). \tag{24}$$

The Dyson equations (21)–(24) are the main result of this section which we will refine only with some minor simplifications. First, there are no correlations on the leads and the corresponding degrees of freedom may be integrated out. Substituting, respectively, (22) in (21), and (24) in (23), yields

$$\begin{aligned}G^r_{\sigma\sigma}(t,t') &= g^r_{0,B}(t,t')\\ &+\int \mathrm{d}t_1\,\mathrm{d}t_2\,g^r_{0,B}(t,t_1)\,\Sigma^r(t_1,t_2)G^r_{\sigma\sigma}(t_2,t')\\ &+U\int \mathrm{d}t_1\,g^r_{0,B}(t,t_1)G^r_{\sigma\sigma,U}(t_1,t')\,,\end{aligned} \tag{25}$$

$$\begin{aligned}G^r_{\sigma\sigma,U}(t,t') &= g^r_{U,B}(t,t')\,n_{\bar\sigma}(t')\\ &+\int \mathrm{d}t_1\,\mathrm{d}t_2\,g^r_{U,B}(t,t_1)\,\Sigma^r(t_1,t_2)\,G^r_{\sigma\sigma,U}(t_2,t')\,,\end{aligned} \tag{26}$$

where $\Sigma^r(t,t_1)$ is the retarded tunneling or hybridization self-energy:

$$\begin{aligned}\Sigma^r(t,t') &= \sum_{k\alpha}V^*_{k\alpha}(t)\,g^r_{k\alpha}(t,t')\,V_{k\alpha}(t')\\ &= -\mathrm{i}\,\theta(t-t')\sum_\alpha\int\frac{\mathrm{d}\varepsilon}{2\pi}\,\mathrm{e}^{-\mathrm{i}\,\varepsilon(t-t')}\,\Gamma^\alpha(\varepsilon,t,t')\,.\end{aligned} \tag{27}$$

Second, we decouple the integral equations (25) and (26): to this end, we operate with the inverse atomic $\mathbf{g}^{-1}_{0(U),B} = [\mathrm{i}\frac{\partial}{\partial t}-\varepsilon_{0(U)}(t)-\mu_B B\sigma]$ from the left and, noticing that $\mathbf{g}^{-1}_{U,B} = \mathbf{g}^{-1}_{0,B} - U$, obtain

$$\begin{aligned}\mathbf{g}^{-1}_{0,B}\,G^r_{\sigma\sigma}(t,t') &= \delta(t-t')\\ &+\int \mathrm{d}t_1\,\Sigma^r(t,t_1)G^r_{\sigma\sigma}(t_1,t')+U\,G^r_{\sigma\sigma,U}(t,t')\end{aligned} \tag{28}$$

and

$$\begin{aligned}\mathbf{g}^{-1}_{0,B}\,G^r_{\sigma\sigma,U}(t,t') &= \delta(t-t')\,n_{\bar\sigma}(t)\\ &+\int \mathrm{d}t_1\,\Sigma^r(t,t_1)G^r_{\sigma\sigma,U}(t_1,t')+U\,G^r_{\sigma\sigma,U}(t,t')\,.\end{aligned} \tag{29}$$

Subtracting (29) from (28) yields two independent Dyson equations, namely (26) and

$$\begin{aligned}G^r_{\sigma\sigma,0}(t,t') &= g^r_{0,B}(t,t')\,[1-n_{\bar\sigma}(t')]\\ &+\int \mathrm{d}t_1\,\mathrm{d}t_2\,g^r_{0,B}(t,t_1)\,\Sigma^r(t_1,t_2)\,G^r_{\sigma\sigma,0}(t_2,t')\,,\end{aligned} \tag{30}$$

where $G_{\sigma\sigma,0}$ is a new auxiliary Green's function defined as

$$G^r_{\sigma\sigma,0}(t,t') = G^r_{\sigma\sigma}(t,t') - G^r_{\sigma\sigma,U}(t,t')\,. \tag{31}$$

And, third and finally, the shorthand notation,

$$\tilde G^r_{\sigma\sigma,0}(t,t') = \frac{G^r_{\sigma\sigma,0}(t,t')}{1-n_{\bar\sigma}(t')} \tag{32a}$$

and

$$\tilde G^r_{\sigma\sigma,U}(t,t') = \frac{G^r_{\sigma\sigma,U}(t,t')}{n_{\bar\sigma}(t')}\,, \tag{32b}$$

rids the zero-tunneling Green's functions in equations (26) and (30) of the prefactors $n_{\bar\sigma}$ and $(1-n_{\bar\sigma})$.

We thus end up with

$$\tilde{G}^r_{\sigma\sigma,0}(t,t') = g^r_{0,B}(t,t') + \int \mathrm{d}t_1\,\mathrm{d}t_2\, g^r_{0,B}(t,t_1)\,\Sigma^r(t_1,t_2)\,\tilde{G}^r_{\sigma\sigma,0}(t_2,t') \quad (33a)$$

and

$$\tilde{G}^r_{\sigma\sigma,U}(t,t') = g^r_{U,B}(t,t') + \int \mathrm{d}t_1\,\mathrm{d}t_2\, g^r_{U,B}(t,t_1)\,\Sigma^r(t_1,t_2)\,\tilde{G}^r_{\sigma\sigma,U}(t_2,t')\,, \quad (33b)$$

which—up to the time-dependent Zeeman shift $\mu_B B(t)\sigma$, present in both atomic $g^r_{0,B}$ and $g^r_{U,B}$, and the 'Coulomb shift' $\varepsilon_0(t) \to \varepsilon_U \equiv \varepsilon_0(t) + U$ affecting only the latter—agree with the Dyson equation for a QD without Coulomb interaction [25].

3.2. Analytic continuation and 'lesser' correlation function

The generalization of our Dyson equations to a non-equilibrium setup is readily obtained by using Langreth's theorem [42, 43]. This produces the usual Keldysh equation for the lesser correlation function,

$$\begin{aligned} G^< &= [1 + G^r\Sigma^r]\; G^<_0\; [1 + \Sigma^a G^a] + G^r\Sigma^< G^a \\ &= G^r\Sigma^< G^a\,, \end{aligned} \quad (34)$$

where time convolutions are implicit. In the first line, the first term on the r.h.s. vanishes [44]: in the Dyson equation for the retarded Green's function, $G^r = [1 + G^r\Sigma^r]\; G^r_0$, the term in brackets equals $G^r\; [G_0]^{-1}$, where the inverse free Green functions can be viewed as operator yielding $\delta(\tau - \tau')$ when applied to the contour-ordered free Green's function G_0. For τ in the upper and τ' in the lower branch of the Keldysh contour we have $G_0 = G^<_0$, and thus $[G_0]^{-1}\; G^<_0 = 0$.

For our purposes, the Keldysh equation (34) becomes

$$\tilde{G}^<_{\sigma\sigma,0(U)}(t,t') = \int \mathrm{d}t_1\,\mathrm{d}t_2\, \tilde{G}^r_{\sigma\sigma,0(U)}(t,t_1)\,\Sigma^<(t_1,t_2)\,\tilde{G}^a_{\sigma\sigma,0(U)}(t_2,t')\,, \quad (35)$$

where $\Sigma^<(t,t')$ is the lesser self-energy

$$\begin{aligned} \Sigma^<(t,t') &= \sum_{k\,\alpha} V^*_{k\alpha}(t)\, g^<_{k\alpha}(t,t')\, V_{k\alpha}(t') \\ &= \mathrm{i}\sum_\alpha \int \frac{\mathrm{d}\omega}{2\pi}\, \mathrm{e}^{-\mathrm{i}\omega(t-t')}\, f_\alpha(\omega)\,\Gamma^\alpha(\omega,t,t')\,. \end{aligned} \quad (36)$$

As usual, the advanced Green's function follows by complex conjugation,

$$\tilde{G}^a_{\sigma\sigma,0(U)}(t,t') = \left[\tilde{G}^r_{\sigma\sigma,0(U)}(t',t)\right]^*\,. \quad (37)$$

Of course, the original dot Green's function can be recovered via

$$G^x_{\sigma\sigma}(t,t') = \tilde{G}^x_{\sigma\sigma,0}(t,t')\;[1 - n_{\bar\sigma}(t')] + \tilde{G}^x_{\sigma\sigma,U}(t,t')\,n_{\bar\sigma}(t')\,, \quad (38)$$

where x may represent $r, a, <$, or $>$. Finally, the time-dependent occupation numbers $n_\sigma(t)$ are obtained self-consistently via

$$n_\sigma(t) = \mathrm{Im}\, G^<_{\sigma\sigma}(t,t)\,. \quad (39)$$

4. Stationary current

In this section, we apply the above results to the special case of a time-independent current through the QD. The more general case of a time-dependent current will be considered in the next section.

A stationary current arises when a constant voltage drop is applied to the leads, and when gate voltage and magnetic field are also time independent. Without explicit time dependence, i.e. with $\frac{\partial}{\partial t}V_{k\alpha}(t) = \frac{\partial}{\partial t}\varepsilon_{k\alpha}(t) = \frac{\partial}{\partial t}\Delta_\alpha(t) = \frac{\partial}{\partial t}B(t) = 0$, all Green's function depend only on the time difference $t - t'$, and the Dyson equations (33) can be solved analytically by Fourier transform, $t - t' \to \omega$.

The retarded (advanced) lead Green's function is given by

$$g^{r(a)}_{k\alpha}(\omega) = \frac{1}{\omega \pm \varepsilon_{k\alpha} \pm i0^+} \quad (40)$$

where the $\pm i0^+$ translates the boundary conditions to the Fourier domain. The retarded, advanced and lesser tunneling self-energy, introduced in equation (27), thus become

$$\begin{aligned} \Sigma^{r(a)}(\omega) &= \sum_{k\alpha} |V_{k\alpha}|^2 g^{r(a)}_{k\alpha}(\omega) \\ &= \left[\Lambda^L(\omega) + \Lambda^R(\omega)\right] \mp \frac{\mathrm{i}}{2}\,\left[\Gamma^L(\omega) + \Gamma^R(\omega)\right] \\ &= \Lambda(\omega) \mp \frac{\mathrm{i}}{2}\,\Gamma(\omega) \end{aligned} \quad (41a)$$

and

$$\begin{aligned} \Sigma^<(\omega) &= \sum_{k\alpha} |V_{k\alpha}|^2 g^<_{k\alpha}(\omega) \\ &= \mathrm{i}\left[\Gamma^L(\omega) f_L(\omega) + \Gamma^R(\omega) f_R(\omega)\right]\,. \end{aligned} \quad (41b)$$

The Dyson equations (33) for the auxiliary functions are now algebraic,

$$\tilde{G}^{r(a)}_{\sigma\sigma,0(U)}(\omega) = g^{r(a)}_{0(U),B}(\omega) + g^{r(a)}_{0(U),B}(\omega)\,\Sigma^{r(a)}(\omega)\,\tilde{G}^{r(a)}_{\sigma\sigma,0(U)}(\omega)\,, \quad (42)$$

and thus readily solved,

$$\tilde{G}^{r(a)}_{\sigma\sigma,0(U)}(\omega) = \frac{1}{\omega - \varepsilon_{0(U)} - \mu_B B\sigma - \Lambda(\omega) \pm \frac{\mathrm{i}}{2}\Gamma(\omega)}\,. \quad (43)$$

Equation (38) brings us back to the original dot Green's function,

$$G^{r(a)}_{\sigma\sigma}(\omega) = \frac{1 - n_{\bar\sigma}}{\omega - \varepsilon_0 - \mu_B B\sigma - \Lambda(\omega) \pm \frac{\mathrm{i}}{2}\Gamma(\omega)} + \frac{n_{\bar\sigma}}{\omega - \varepsilon_U - \mu_B B\sigma - \Lambda(\omega) \pm \frac{\mathrm{i}}{2}\Gamma(\omega)}\,. \quad (44)$$

The corresponding spectral function

$$A_\sigma(\omega) = \mathrm{i}\left[G^r_{\sigma\sigma}(\omega) - G^a_{\sigma\sigma}(\omega)\right] \tag{45}$$

$$= \Gamma(\omega)\left[\frac{1-n_{\bar\sigma}}{\left[\omega-\varepsilon_0-\mu_B B\sigma-\Lambda(\omega)\right]^2+\left[\frac{1}{2}\Gamma(\omega)\right]^2} + \frac{n_{\bar\sigma}}{\left[\omega-\varepsilon_U-\mu_B B\sigma-\Lambda(\omega)\right]^2+\left[\frac{1}{2}\Gamma(\omega)\right]^2}\right] \tag{46}$$

enables us to write the lesser function as

$$G^<_{\sigma\sigma}(\omega) = \mathrm{i}A_\sigma(\omega)\,\frac{\left[\Gamma^L(\omega)f_L(\omega)+\Gamma^R(\omega)f_R(\omega)\right]}{\Gamma(\omega)}\,, \tag{47}$$

and equation (39) for the occupation numbers as

$$n_\sigma = \int \frac{\mathrm{d}\omega}{2\pi} A_\sigma(\omega)\,\frac{\left[\Gamma^L(\omega)f_L(\omega)+\Gamma^R(\omega)f_R(\omega)\right]}{\Gamma(\omega)}\,. \tag{48}$$

In the stationary case, the self-consistent solution of the latter equation may be obtained analytically and reads

$$n_\sigma = \frac{n^0_\sigma - n^0_\sigma(n^0_\sigma - n^U_\sigma)}{1-(n^0_\sigma-n^U_\sigma)(n^0_{\bar\sigma}-n^U_{\bar\sigma})}\,, \tag{49}$$

where

$$n^{0(U)}_\sigma = \int \frac{\mathrm{d}\omega}{2\pi}\,\frac{\Gamma^L(\omega)f_L(\omega)+\Gamma^R(\omega)f_R(\omega)}{\left[\omega-\varepsilon_{0(U)}-\mu_B B\sigma-\Lambda(\omega)\right]^2+\left[\frac{1}{2}\Gamma(\omega)\right]^2}\,. \tag{50}$$

Finally, the explicit time dependence of the current in equation (8) vanishes since we may integrate over t_1 (see [25]), yielding

$$\begin{aligned} J_{L(R)} &= -\frac{e}{\hbar}\int\frac{\mathrm{d}\varepsilon}{2\pi}\sum_\sigma \Gamma^{L(R)}(\varepsilon) \\ &\quad\times\left\{G^<_{\sigma\sigma}(\varepsilon) + f_{L(R)}(\varepsilon)\left[G^r_{\sigma\sigma}(\varepsilon)-G^a_{\sigma\sigma}(\varepsilon)\right]\right\} \\ &= -\frac{e}{\hbar}\int\frac{\mathrm{d}\varepsilon}{2\pi}\sum_\sigma \frac{\Gamma^L(\varepsilon)\,\Gamma^R(\varepsilon)}{\Gamma(\varepsilon)} \\ &\quad\times\left[f_{R(L)}(\varepsilon)-f_{L(R)}(\varepsilon)\right]\,A_\sigma(\varepsilon)\,. \end{aligned} \tag{51}$$

Note that the results of this section are exact in the non-interacting limit (where $U\to 0$), as well as in the atomic limit (where $V_{k\alpha}\to 0$) for any value of the magnetic field B.

5. Time-dependent current

In this section, we analyze the time-dependent current through the QD. For metallic contacts, it is generally safe to assume that the details of the band structure are of little importance, and that both leads may be represented by a constant and infinitely wide density of states, i.e. $\rho(\varepsilon) = \text{const}$—an approximation commonly referred to as 'wide-band limit[5]' Further simplifications arise if we assume the tunneling between the dot and the leads to be the same for all lead states, i.e. $V_{k\alpha}(t) = u_\alpha(t)V_\alpha$, with the time dependence residing solely in a overall function, $u_\alpha(t)$, characteristic of each lead.

With these approximations, the barrier functions (9) become independent of ε,

$$\Gamma^\alpha(t_1,t) = 2\pi\rho\,u_\alpha(t)u_\alpha(t_1)|V_\alpha|^2\exp\left[\mathrm{i}\int_{t_1}^t \mathrm{d}t_2\Delta_\alpha(t_2)\right]\,. \tag{52}$$

Via the Fourier transform in (27), this produces an instantaneous tunneling self-energy,

$$\Sigma^r(t,t') = -\frac{\mathrm{i}}{2}\,\Gamma(t)\delta(t-t')\,, \tag{53}$$

where $\Gamma(t) = \sum_\alpha \Gamma^\alpha(t,t) = 2\pi\rho\,\sum_\alpha u^2_\alpha(t)|V_\alpha|^2$. Moreover, we define $\Gamma^\alpha = 2\pi\rho\,|V_\alpha|^2$, and write $\Gamma(t) = \sum_\alpha \Gamma^\alpha u^2_\alpha(t)$ henceforth.

The δ-function in Σ^r enables us to do one of the two time integrations in the Dyson equations (33) for the auxiliary Green's functions,

$$\begin{aligned} \tilde G^r_{\sigma\sigma,0(U)}(t,t') &= g^r_{0(U),B}(t,t') \\ &\quad -\frac{\mathrm{i}}{2}\int \mathrm{d}t_1\, g^r_{0(U),B}(t,t_1)\,\Gamma(t_1)\,\tilde G^r_{\sigma\sigma,0(U)}(t_1,t')\,. \end{aligned} \tag{54}$$

The solution of the latter equation are just the atomic Green's functions broadened by the finite tunneling life-time,

$$\tilde G^r_{\sigma\sigma,0(U)}(t,t') = g^r_{0(U),B}(t,t')\,\exp\left[-\frac{1}{2}\int_{t'}^t \Gamma(t_1)\mathrm{d}t_1\right]\,, \tag{55}$$

from which the original dot Green's function are recovered via equation (38),

$$\begin{aligned} G^r_{\sigma\sigma}(t,t') &= \left[g^r_{0,B}(t,t')\left[1-n_{\bar\sigma}(t')\right] + g^r_{U,B}(t,t')n_{\bar\sigma}(t')\right] \\ &\quad\times\exp\left[-\frac{1}{2}\int_{t'}^t\Gamma(t_1)\mathrm{d}t_1\right]\,. \end{aligned} \tag{56}$$

Again, the dot occupation is obtained from the imaginary part of the lesser Green's function at equal times [see equation (39)], yielding

$$\begin{aligned} n_\sigma(t) &= \sum_\alpha \Gamma^\alpha\int\frac{\mathrm{d}\omega}{2\pi}f_\alpha(\omega) \\ &\quad\times\left[\left[1-n_{\bar\sigma}(t)\right]\left|A^0_{\alpha,\sigma}(\omega,t)\right|^2 + n_{\bar\sigma}(t)\left|A^U_{\alpha,\sigma}(\omega,t)\right|^2\right] \end{aligned} \tag{57}$$

where

$$\begin{aligned} A^{0(U)}_{\alpha,\sigma}(\omega,t) &= \int_{-\infty}^t \mathrm{d}t_1\,u_\alpha(t_1)\,\tilde G^r_{\sigma\sigma,0(U)}(t,t_1) \\ &\quad\times\exp\left[\mathrm{i}\omega(t-t_1) + \mathrm{i}\int_{t_1}^t \mathrm{d}t_2\,\Delta_\alpha(t_2)\right] \end{aligned} \tag{58}$$

denote the corresponding spectral functions.

Equation (57) defines a system of linear equations for n_σ and $n_{\bar\sigma}$ which, introducing the shorthand

$$n^{0(U)}_\sigma(t) = \sum_\alpha \Gamma^\alpha\int\frac{\mathrm{d}\omega}{2\pi}f_\alpha(\omega)\left|A^{0(U)}_{\alpha,\sigma}(\omega,t)\right|^2\,, \tag{59}$$

[5] In the opposite case of extremely narrow contact bands, the continua in the conductance are expected to be accompanied by additional peaks and side-bands [45–47].

may be written as

$$n_\sigma(t) = [1 - n_{\bar\sigma}(t)]\; n^0_\sigma(t) + n_{\bar\sigma}(t)\, n^U_\sigma(t)\;. \tag{60}$$

Its solution is the same as in the stationary case, equation (49), albeit now with time-dependent n^0_σ and n^U_σ.

With the notation

$$B^0_{\alpha,\sigma}(\omega,t) = \int_{-\infty}^{t} \mathrm{d}t_1\; [1 - n_{\bar\sigma}(t_1)]\; u_\alpha(t_1)\, \tilde G^r_{\sigma\sigma,0}(t,t_1) \exp\left[\mathrm{i}\omega(t-t_1) + \mathrm{i}\int_{t_1}^{t} \mathrm{d}t_2 \Delta_\alpha(t_2)\right], \tag{61a}$$

$$B^U_{\alpha,\sigma}(\omega,t) = \int_{-\infty}^{t} \mathrm{d}t_1\, n_{\bar\sigma}(t_1)\, u_\alpha(t_1)\, \tilde G^r_{\sigma\sigma,U}(t,t_1) \exp\left[\mathrm{i}\omega(t-t_1) + \mathrm{i}\int_{t_1}^{t} \mathrm{d}t_2 \Delta_\alpha(t_2)\right]. \tag{61b}$$

the current from the leads to the dot, given by equation (8), can be expressed in the wide-band limit as

$$J_\alpha(t) = -\frac{e}{\hbar}\,\Gamma^\alpha u^2_\alpha(t) \sum_\sigma \left[n_\sigma(t) + \int \frac{\mathrm{d}\omega}{\pi} f_\alpha(\omega)\, \mathrm{Im}\left[B^0_{\alpha,\sigma}(\omega,t) + B^U_{\alpha,\sigma}(\omega,t)\right]\right]. \tag{62}$$

The contribution proportional to the dot occupation in the first line describes the current from the dot to the lead and stems from the lesser Green's function (for which both integrations in (8) can be evaluated due to the energy independence of the barrier functions). The second line in (62) is produced by the retarded Green's function in (8) and represents the current in the inverse direction: the term involving $B^0_{\alpha,\sigma}$ represents tunneling from the lead α to an empty dot, and the term with $B^U_{\alpha,\sigma}$ to an already $\bar\sigma$-occupied dot.

6. Numerical results

In the previous two sections, we derived expressions for the current J_α from the leads to the dot for the stationary case, equation (51), and for the wide-band limit of the time-dependent regime, equation (62). In both cases, the dot occupation number is given by the analytical expression (49), such that the aforementioned equations for J_α depend ultimately only on integrals over known functions and no iteration procedure to self-consistency is needed. Details of the numerical method may be found in appendix.

Here, we calculate the current J_α numerically for the case of leads characterized by a constant and infinitely wide density of states, and where each lead state offers the same tunneling probability to the dot. In this case, equation (53) produces a tunneling self-energy $\Sigma^r(t,t') = -\frac{\mathrm{i}}{2}\sum_\alpha \Gamma^\alpha \delta(t-t')$ with constant Γ^α which, after Fourier transformation, yields

$$\Lambda^\alpha(\omega) \equiv 0 \quad \text{and} \quad \Gamma^\alpha(\omega) \equiv \Gamma^\alpha\;. \tag{63}$$

Henceforth, we will use the combined tunneling to both leads, $\Gamma = \sum_\alpha \Gamma^\alpha$, as our energy unit.

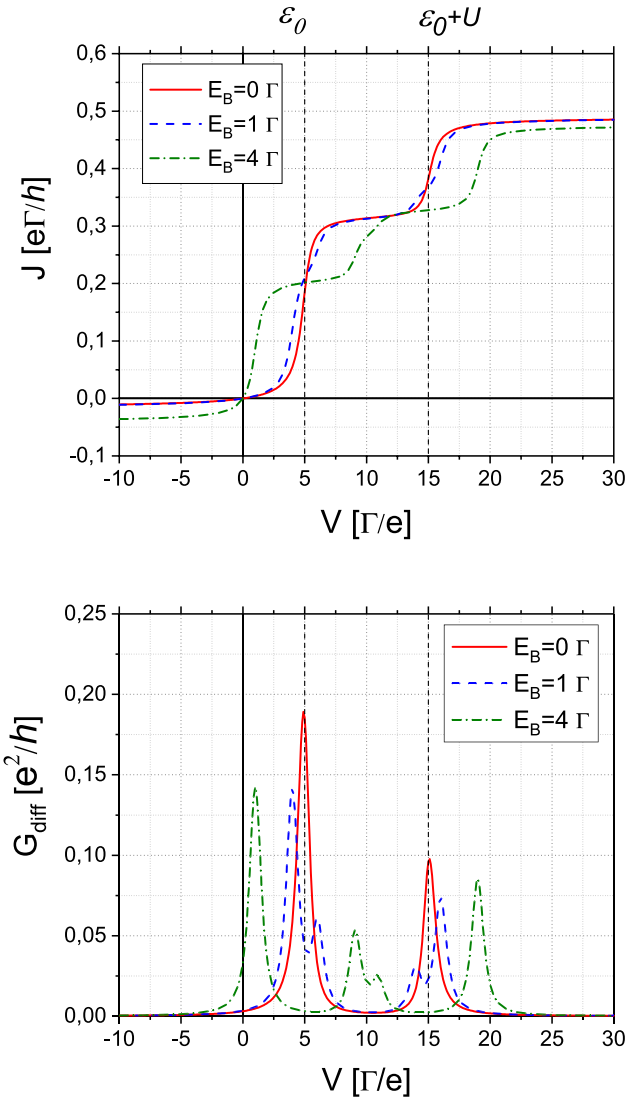

Figure 2. Stationary current through the dot (upper panel) and corresponding differential conductance (lower panel) as a function of bias voltage. Parameters are $\mu_L = eV$, $\mu_R = 0\,\Gamma$, $\varepsilon_0 = 5\,\Gamma$, $U = 10\,\Gamma$. Solid (red), dashed (blue) and dot-dashed (green) lines represent magnetic fields $B = 0, 1$ and $4\,\Gamma/\mu_B$, respectively.

In the first part of this section, we will examine the current through the dot in the stationary regime, where the system is exposed to a constant bias voltage, $eV = \mu_L - \mu_R$, and a constant magnetic field (expressed in terms of its energy equivalent $E_B = \mu_B B$). Thereafter, time dependence will be studied by applying simultaneous voltage and magnetic pulses to formerly unperturbed systems. All calculations will be performed for symmetric barriers, $\Gamma^L = \Gamma^R = \frac{1}{2}\Gamma$, and at temperature $T = 0.1\,\Gamma$. The system will be driven out of equilibrium by applying a voltage to the left lead, and by modifying the dot energy level and magnetic field. The right lead, by contrast, will remain at $\mu_R = 0$ and $\Delta_R(t) = 0$ at all times, thus serving as ground.

Let us first study the stationary regime by applying a constant bias to a QD characterized by $\varepsilon_0 = 5\,\Gamma$ and $U = 10\,\Gamma$. For these parameters, Haldane's expression for the Kondo scale (1) evaluates to $E_K \simeq 2.4 \cdot 10^{-5}\,\Gamma$ which is well below our

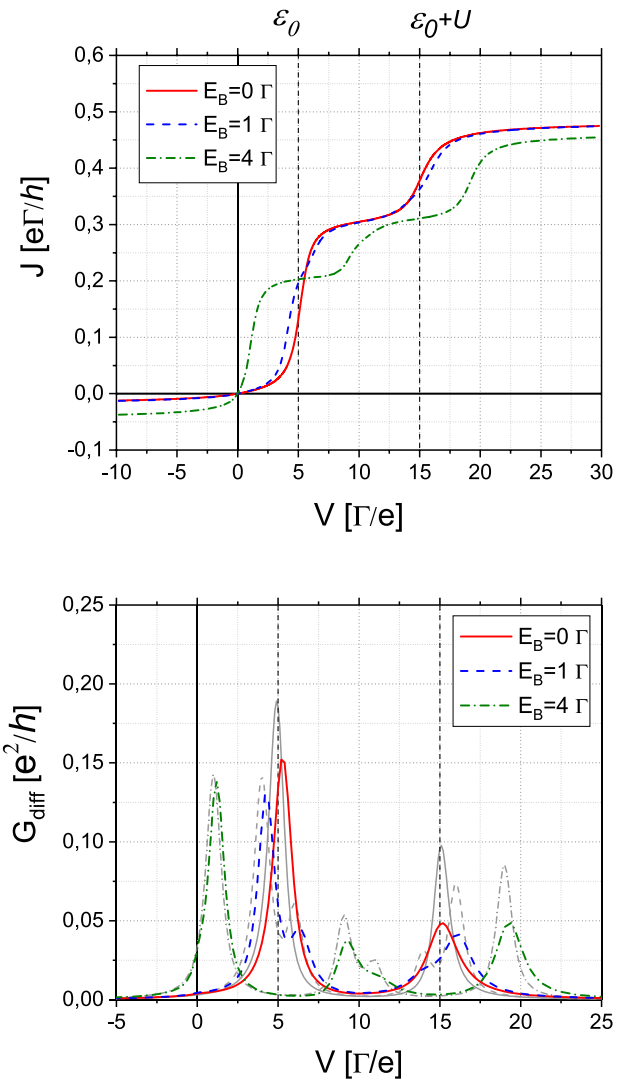

Figure 3. NCA stationary current and differential conductance calculated for the same parameters as in figure 2. For comparison, our extended Hubbard I results from figure 2 are shown as faint gray lines in the lower panel.

choice of temperature, $T = 0.1\,\Gamma$. Therefore, even in absence of a magnetic field, our setup is well outside the Kondo regime. Figure 2 shows the symmetrized currents through the dot, $J = \frac{1}{2}(J_L - J_R)$, and the corresponding differential conductances, $G_{\text{diff}} = \mathrm{d}J/\mathrm{d}V$, as functions of the bias voltage $\mu_L = eV$ for different values of the magnetic field, and figure 3 shows the corresponding NCA results. It can be seen that both methods produce very similar results predicting, as expected, a current rising stepwise with increasing voltage. Moreover, the step positions and heights of both methods agree. Although the NCA is capable of tackling the Kondo regime, its differential conductances exhibit no sharp resonances, thus corroborating our previous analysis that Kondo physics is unimportant in the parameter range under investigation.

Without a magnetic field (solid red lines), the first step arises when eV reaches ε_0 and the thus far empty dot level becomes energetically available for tunneling processes from the left lead. Such processes occur, of course, with equal probability for both spin species, and represent therefore two conduction channels. For $eV > \varepsilon_0$, these channels remain open, resulting in a dot which alternates between the empty and singly occupied configuration. For $eV > \varepsilon_0 + U$, the Coulomb repulsion on the dot can be overcome, and a second electron may be hosted by an already singly occupied dot. But the latter process represents only one additional conduction channel since the other is blocked by the Pauli principle. Therefore, the second step of the solid red current curve in the upper panel of figure 2, at $\varepsilon_0 + U = 15\,\Gamma$, is only half the height of the first, at $\varepsilon_0 = 5\,\Gamma$. In the differential conductance or density of states, shown in the lower panel, this gives rise to a lower Hubbard band at ε_0 with twice the spectral weight of the upper Hubbard band at $\varepsilon_0 + U$. At sufficiently low temperature, the width of both Hubbard bands is essentially governed by the tunneling matrix elements and thus given by Γ.

The NCA results shown in figure 3 confirm this spectral weight asymmetry. Such asymmetries have also been observed under equilibrium conditions in related models with strong electron correlations [39, 40] where the weight transfer occurs as a function of the Fermi energy. A detailed comparison of the NCA differential conductances to extended Hubbard I, represented by gray lines in figure 3, shows that both methods essentially agree on the shape of the lower Hubbard bands, while the NCA produces generally softer upper Hubbard bands. These findings persist for non-vanishing magnetic fields and might be due to the fact that the NCA encompasses some of the spin dynamics neglected in the extended Hubbard I approximation. However, the benchmark of both methods against QMC (further on in this section) seems to indicate conversely that the rendering of the dynamics in our method is somewhat superior to the NCA.

For non-vanishing magnetic fields, the situation remains similar, although the energetically favored $\downarrow$-spin level will be accessible before its $\uparrow$-spin counterpart. Therefore, each of the aforementioned current steps is split into two sub-steps, occurring at $\pm E_B$ relative to the position without magnetic field. This Zeeman splitting is most obvious in the differential conductance for $E_B = 1\,\Gamma$ represented by the dashed blue line in the lower panel of figure 2. For $E_B = 4\,\Gamma$, shown as dot-dashed green lines, the splitting is much larger : the Zeeman components of the lower Hubbard band occur at $\varepsilon_0 - E_B = 1\,\Gamma$ and $\varepsilon_0 + E_B = 9\,\Gamma$, and those of the upper Hubbard band at $\varepsilon_0 + U - E_B = 11\,\Gamma$ and $\varepsilon_0 + U + E_B = 19\,\Gamma$.

Note that for both of our magnetic field values, $E_B = 1$ and $4\,\Gamma$, the splitting between the closest levels is only $2\,\Gamma$ and thus too small to produce neat current sub-steps in the upper panel of figure 2. The differential conductance in the lower panel, by contrast, resolves all features clearly.

We now turn to the time-dependent regime. At first, we will benchmark our method against recent diagrammatic QMC results obtained with the so-called inchworm algorithm developed by G. Cohen *et al* [30] with which they investigated the time evolution of the population difference on the dot, $\Delta P = n_\uparrow - n_\downarrow$, after a coupling quench with $U = 8\Gamma$. Here, we set up analogous initial conditions: we start from a fully polarized state, obtained with a large magnetic field, $B = 90\,\Gamma/\mu_B$, which is switched off at $t = 0$. As shown in

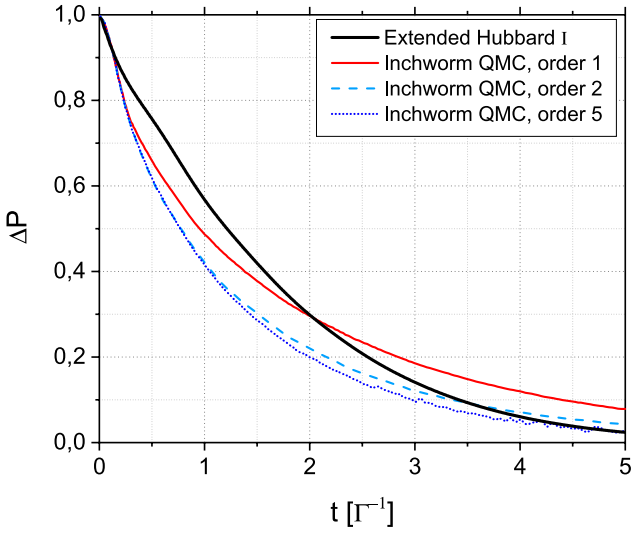

Figure 4. Relaxation from the fully polarized to a non-magnetic state in the mixed valence regime, for parameters $\varepsilon_0 = -0.5\,\Gamma$ and $U = 8\,\Gamma$. Extended Hubbard I (solid black line) compared to different orders of diagrammatic 'inchworm' QMC (solid red, dashed light blue and dotted dark blue lines). Inchworm data from figure 3 of [30].

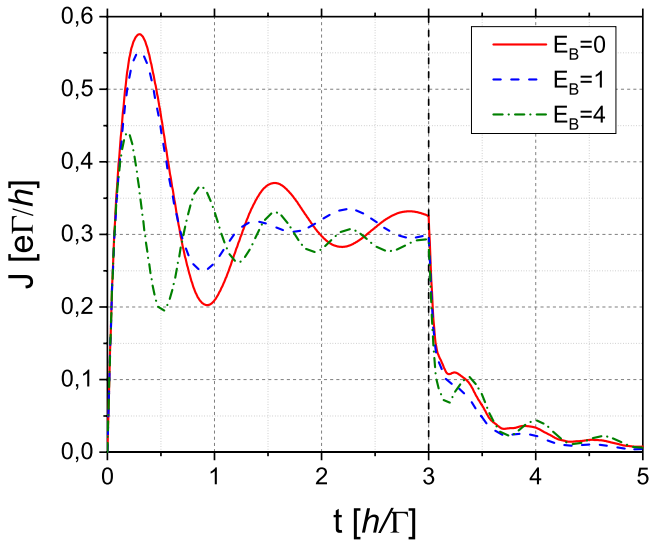

Figure 5. Time dependence of the symmetrized current through a QD perturbed by simultaneous voltage and magnetic pulses between $t = 0$ and $t_{\text{pulse}} = 3\,\hbar/\Gamma$. Without pulse, the system is characterized by $\mu_L = \mu_R = 0\,\Gamma$, $\varepsilon_0 = 0\,\Gamma$, and $U = 10\,\Gamma$. During the rectangular pulse, the left lead levels are increased by $\Delta_L = 10\,\Gamma$, and the dot level by $\Delta = 5\,\Gamma$. Solid (red), dashed (blue) and dot-dashed (green) lines represent magnetic pulse values of $B = 0, 1$ and $4\,\Gamma/\mu_B$, respectively.

figure 4, our method (continuous black line) reproduces the overall shape and time-dependence of the relaxation to a non-magnetic state predicted by Cohen's inchworm QMC. Even if some quantitative differences subsist at intermediate time scales, it becomes obvious that our method—in contrast to most other purely numerical methods discussed by Cohen *et al* [30]—is perfectly stable and produces meaningful results in the long time limit. Acknowledging the fact that the *n*th order of the inchworm QMC algorithm corresponds approximately to an $n-1$-crossing approximation, [30] it can be seen from the figure that the extended Hubbard I approximation outperforms the first order inchworm (which would correspond to NCA) for longer times, and captures some of the dynamics encompassed only by higher orders of the inchworm scheme.

We now investigate an experimentally more interesting time-dependent setup where an unperturbed system, given by $\mu_L = \mu_R = \varepsilon_0 = 0\,\Gamma$, is driven out of equilibrium by a simultaneous voltage and magnetic pulse. The pulse is of rectangular shape, i.e. $\Delta_L(t) = 10\,\Gamma$ and $\Delta(t) = 5\,\Gamma$ are added to the energy levels of, respectively, the left lead and the dot, while the right lead remains grounded, $\mu_R = \Delta_R(t) = 0\,\Gamma$. Also, for the duration of the voltage pulse, a magnetic field is switched on. The parameters are such that, during the pulse, the system is exposed to the same physical conditions as for bias $eV = 10\,\Gamma$ in the stationary regime studied above.

As illustrated in figure 5, the current starts with the onset of the pulse at $t = 0$. $J(t)$ would then eventually recover the corresponding stationary value in a damped oscillation governed by $\exp(-\Gamma t)$. The damping timescale is given by the inverse tunneling Γ^{-1}, which is the same for all magnetic fields, but the details of the oscillations and the value of the stationary current depend on the field. From figure 5, we find roughly $J_{\text{stat}} \simeq 0.3\,e\Gamma/\hbar$ for $E_B = 0$ and $1\,\Gamma$, and slightly less for $E_B = 4\,\Gamma$, in agreement with the values for $J(eV = 10\,\Gamma)$ from figure 2. In our setup, however, the pulse is switched off before the stationary state is fully reached, at $t_{\text{pulse}} = 3\,\hbar/\Gamma$. Thereafter, the system oscillates back to its original equilibrium.

Figure 6 shows the overall (three upper curves) and spin-resolved (lower curves) dot occupancies for $E_B = 0$,1 and $4\,\Gamma$. Clearly, in absence of the pulse and for $\varepsilon_0 = 0$, three configurations are degenerate: the empty, the $\uparrow$- and the $\downarrow$-occupied dot occur with equal probability, thus explaining an equilibrium occupancy of 2/3. We may convince ourselves that in absence of a magnetic field, this equilibrium state is still a valid solution after the onset of the voltage pulse, and as a result, the corresponding red curves remain on their equilibrium values.

For moderate magnetic fields, e.g. $E_B = 1\,\Gamma$ shown as blue curves in figure 6, the pulse drives the system temporarily out of equilibrium. The spin-resolved occupancies then recover their equilibrium value in a damped oscillation with the overall occupancy remaining constant due to the phase shift of π between $\uparrow$ and $\downarrow$-occupancies.

For $E_B = 4\,\Gamma$ shown as yellow and green curves in the figure, the deviation is much stronger and, more importantly, the asymptotically emerging perturbed equilibrium is different from the unperturbed state: at the imposed $eV = 10\,\Gamma$, the $\downarrow$-spin Zeeman component of the upper Hubbard band is found at $E = 11\,\Gamma$ (see figure 2) and thus becomes partially available for transport. Therefore, the spin-resolved occupancies deviate considerably from their unperturbed values, even if the net effect in the total occupancy is rather small.

We now turn to the oscillatory behavior of the currents. It is already obvious from the current curves in figure 5 that the period of the damped oscillations is affected by the magnetic field. Fourier transformation is, of course, a much better tool

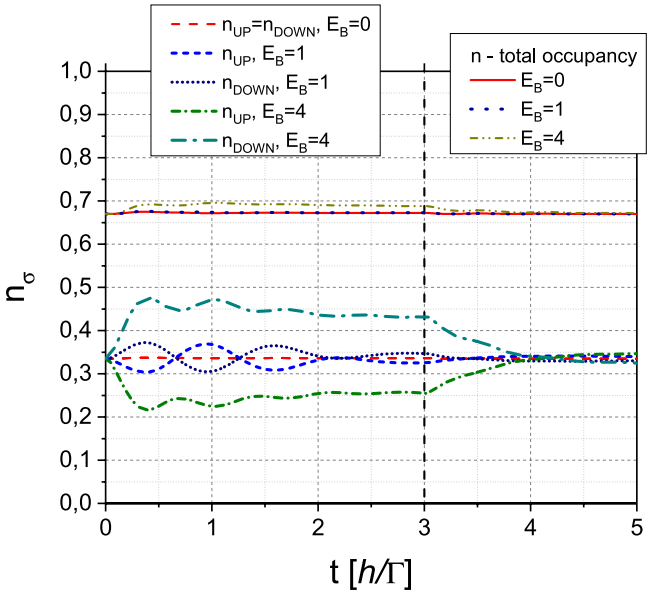

Figure 6. Time dependence of the overall (upper curves) and spin-resolved (lower curves) dot occupancy for a QD governed by the same parameters as in figure 5, i.e. exposed to simultaneous rectangular voltage and magnetic pulses between $t = 0$ and $t_{\text{pulse}} = 3\,\hbar/\Gamma$. Solid (red), dashed/dotted (blue) and dot-dashed (green) lines represent magnetic pulse values of $B = 0, 1$ and $4\,\Gamma/\mu_B$, respectively.

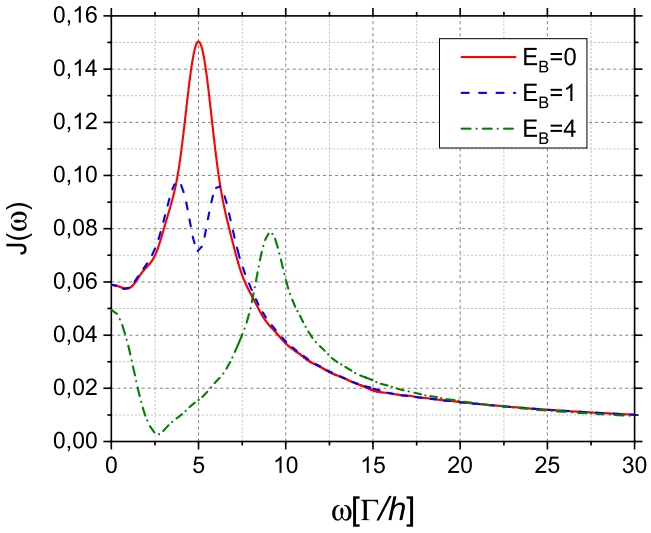

Figure 7. Fourier transform of the time-dependent current through the dot for the same parameters as in figure 5, except for the pulse length which here is $t_{\text{pulse}} = 10\,\hbar/\Gamma$.

to study this in detail: figure 7 shows the currents in the frequency domain for the parameters that were used in figure 5, except for the pulse length which now is $t_{\text{pulse}} = 10$ instead of $3\,\hbar/\Gamma$. The longer pulse was chosen for the oscillations to fade out completely, thus producing much nicer Fourier signals. As can be seen from figure 7, the Fourier transformed currents $J(\omega)$ map out the lower Hubbard band, at $\varepsilon_0 = 5\,\Gamma$, including the Zeeman splitting for non-vanishing magnetic fields. The intensity of the peaks in $J(\omega)$, however, does not match the weights in the density of states—a fact which is of no surprise since Fourier transformation does not conserve areas under functions but rather integrals over squared functions as in Plancharel's theorem.

Note that the upper Hubbard band is absent from the figure since, as pointed out before, double occupancies involve an energy cost too high for a bias voltage of $eV = 10\,\Gamma$ (except for $E_B = 4\,\Gamma$ where the lower Zeeman component of the upper Hubbard band, centered at $E = 11\,\Gamma$, can be partially addressed).

Finally, we study a setup where, between $t = 0$ and $t_{\text{pulse}} = 10\,\hbar/\Gamma$, a rectangular voltage pulse of $\Delta_L = 20\,\Gamma$ and a magnetic pulse of $B = 1\,\Gamma/\mu_B$ are applied to a QD formerly in an equilibrium characterized by $\mu_L = \mu_R = \varepsilon_0 = 0\,\Gamma$. In this setup the doubly occupied dot level becomes energetically available, and all transport channels are open. Therefore, $J(t)$ in the top panel of figure 8 saturates around $\frac{1}{2}\,e\Gamma/\hbar$ instead of the $\frac{1}{3}\,e\Gamma/\hbar$ observed in figure 5. When the pulse is on, tunneling from the left lead to an empty dot releases an energy of $\Delta_L - \varepsilon_0 - \Delta - \sigma\mu_B B$ which amounts to $16\,\Gamma$ for $\uparrow$- and $18\,\Gamma$ for $\downarrow$-electrons, thus producing very prominent peaks in the Fourier transformed J_L (represented by the dotted blue line in figure 8). Similarly, tunneling from the left lead to an already singly occupied dot releases $\Delta_L - \varepsilon_0 - \Delta - U - \sigma\mu_B B$, but the Fourier transformed J_L shows only a very weak disturbance around the expected values of 6 and $8\,\Gamma$. This suggests that the current involving the now available doubly occupied dot configuration is mainly stationary and contributes only little to the dynamics. The analysis of the current between the dot and the right lead corroborates this interpretation: according to the spin species, the singly-occupied dot level is $\varepsilon_0 + \Delta + \sigma\mu_B B - \Delta_R = 4$ or $2\,\Gamma$ higher in energy than the right lead and produces the clearly visible structure in the Fourier transformed J_R (dashed green curve in figure 8). By contrast, almost no Fourier signal is found from the doubly occupied level around the expected 12 or $14\,\Gamma$.

A supplementary calculation (not shown in the figure) for the same parameters but with $U = 50\,\Gamma$, further supports the idea of mainly stationary transport through the upper Hubbard band: for $U = 50\,\Gamma$, where the doubly occupied dot is unattainable, the time dependence of $J(t)$ is almost identical to the $U = 10\,\Gamma$ case, but oscillates around $\frac{1}{3}\,e\Gamma/\hbar$ instead of the $\frac{1}{2}\,e\Gamma/\hbar$.

The low-frequency behavior of the currents $J_\alpha(\omega)$ in figure 8 is dominated by strong peaks that result from the saturating currents. Assuming a smooth $1 - \exp(-\Gamma t)$-like rise underlying the current oscillations in the top panel produces a Fourier transform of Lorentzian shape peaked at $\omega = 0$ as observed in the low-frequency sector of the bottom panel.

Thus far, we focused on the contributions to the time-dependent current in equation (62) involving $B^{0(U)}_{\alpha,\sigma}$ which describe the current to the dot and are very sensitive to energy differences. There are, however, also terms acknowledging the current flow away from the dot. These are directly proportional to the dot occupancy $n(t)$. Especially for the right lead, the latter contributions will play an important role and are most likely responsible for the rest of features of $J_R(\omega)$ in figure 8.

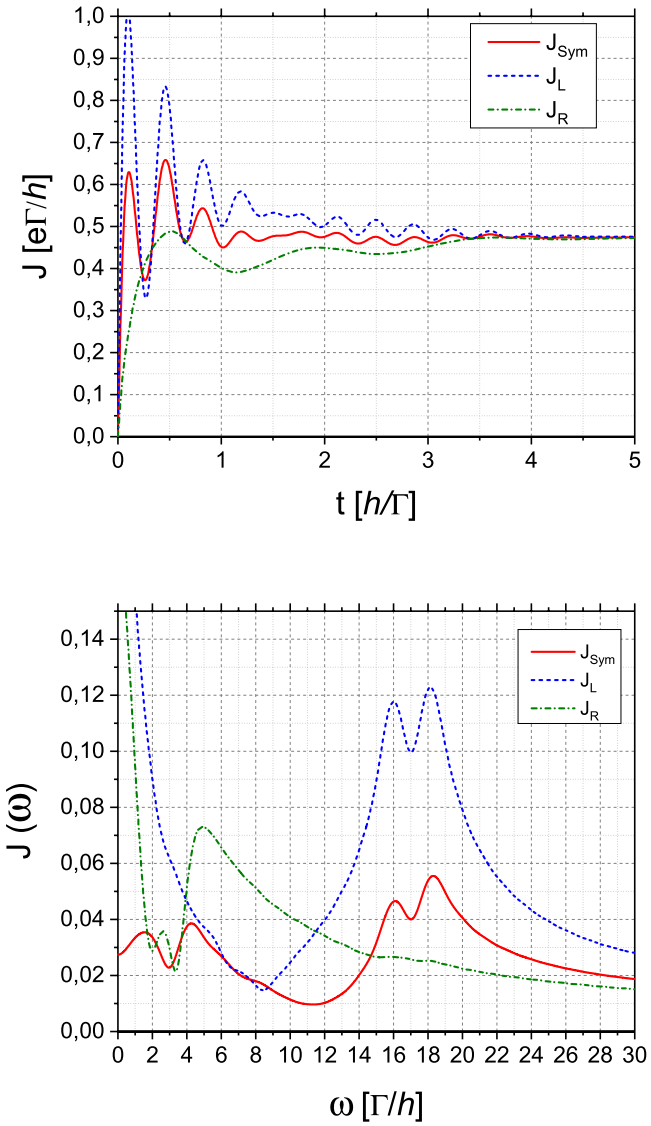

Figure 8. Time-dependent current (upper panel) and its Fourier transform (lower panel) for a QD perturbed by simultaneous voltage and magnetic pulses between $t = 0$ and $t_{\text{pulse}} = 10\,\hbar/\Gamma$. Without pulse, the system is characterized by $\mu_L = \mu_R = 0\,\Gamma$, $\varepsilon_0 = 0\,\Gamma$, and $U = 10\,\Gamma$. During the rectangular pulse, the left lead levels are increased by $\Delta_L = 20\,\Gamma$, the dot level by $\Delta = 3\,\Gamma$, and the magnetic field is $B = 1\,\Gamma/\mu_B$. The solid (red) line represents the symmetrized current through the dot, the dashed (blue) and dot-dashed (green) lines the currents between the dot and, respectively, the left and the right lead.

7. Conclusion

In the present paper, we studied the electronic transport through a single-orbital QD with a strong on-site Coulomb repulsion. The dot is addressed by two uncorrelated metallic leads and may be exposed to an applied magnetic field. Our investigation encompasses setups with constant voltage biases between the leads and a constant magnetic field on the dot, yielding stationary currents, and situations where the system is perturbed by pulsed voltage biases and magnetic fields, producing time-dependent responses.

The electric transport was investigated via non-equilibrium Green's functions in the Keldysh formalism. Our methods are similar to those put forward by Jauho *et al* [25] but, in contrast to the latter, encompass an applied magnetic field, and more importantly, correlations due to the on-site Coulomb U. In this case, no exact solutions are available. Here, we opted for an approximation put forward by some of the authors in a previous paper [36]: the underlying Green's function decoupling scheme bears many similarities with the so-called Hubbard-I approximation, but captures some of the dynamics not encompassed by the latter. In the present paper, we adapt the method to situations where the dot is subject to a non-zero magnetic field. The presentation also includes a pictorial representation of the equations of motion which helps to understand the underlying physical processes.

Well suited for large U, our non-canonical or extended Hubbard-I scheme, is exact in the atomic limit, where the tunneling matrix elements between dot and leads vanish. Moreover, it is also exact in the limit of vanishing Coulomb U on the dot level for any magnetic field.

After integrating out the degrees of freedom of the leads, the decoupling scheme produces a closed system, equations (25) and (26), that has to be solved self-consistently. In the two situations studied in this paper, namely (i) the time-independent setup with constant magnetic field and voltage bias, and (ii) the time-dependent setup with leads of constant and infinitely wide density of states, no iteration procedure is needed and an explicit solution in terms of integrals over ultimately known functions can be stated: these are expressions (51) and (62), respectively, for case (i) and (ii).

The numerical evaluation of the latter yields, in the stationary setup, the expected stepwise rise of the current through the dot with the first step stemming from the transport through the previously unoccupied dot, and the second from tunneling through an already occupied level which, of course, involves overcoming the Coulomb U. More importantly, for an already occupied dot, the Pauli principle blocks one of the spin species and thus the second step only contributes half as much to the conductance as the first. In presence of a magnetic field, the Zeeman effect splits each of the steps into two smaller sub-steps. These findings are supported by an independent NCA calculation.

In the time-dependent regime, we showed that our method reproduces in essence the dynamics of the population relaxation after a quench observed in recent inchworm QMC results [30]. We then turned to the more challenging time-dependent setup where the QD is driven out of equilibrium by simultaneous rectangular voltage and magnetic pulses. After the onset of the pulses, the current through the dot converges to a new equilibrium in a damped oscillation. The precise nature of these oscillations was examined by Fourier analysis. As expected, it revealed that the oscillations are governed by energy level differences, and thus implicitly by the magnetic field. More importantly, Fourier analysis allowed us to show which electronic configurations contribute to the dynamics and which leave mainly a stationary signature in the transport signal.

One major benefit of our method is to suggest an explanation for the physical origin of each peak in the spectrum. For example, we found to our surprise that, for the parameters

chosen, the dynamics of the current is mainly governed by tunneling through the empty dot, while the transport involving a temporarily doubly occupied level contributes mostly to the stationary part of the conductance.

Acknowledgments

The authors would like to express their gratitude to Volodymyr Vovchenko for his expertise and for providing an independent cross check of some of the present numerical results with his computer code. We would also like to thank Anne-Marie Daré for interesting discussions.

D Anchishkin and D Zhuravel acknowledge support from 'The structure and dynamics of statistical and quantum-field systems' program of the Department of Physics and Astronomy of the National Academy of Science of Ukraine.

Appendix. Numerical procedure

The time-dependent current and dot occupancies are essentially determined by the functions $A^{0(U)}_{L/R,\,\sigma}(\omega,t)$ and $B^{0(U)}_{L/R,\,\sigma}(\omega,t)$, equations (58) and (61), which may be written as

$$A^{0(U)}_{\alpha,\sigma}(\omega,t) = -\,\mathrm{i}\int_{-\infty}^{t} \mathrm{d}t_1\, u_\alpha(t_1) \times \exp\left[\mathrm{i}\int_{t_1}^{t} \mathrm{d}t_2\, F^{0(U)}_{\alpha,\sigma}(\omega,t_2)\right] \tag{A.1}$$

where the function

$$F^{0(U)}_{\alpha,\sigma}(\omega,t_2) = \omega - \varepsilon_{0(U)} - \Delta(t_2) - \mu_B B\sigma + \Delta_\alpha(t_2) + \frac{\mathrm{i}}{2}\Gamma(t_2) \tag{A.2}$$

contains all the dynamics of the 'tunneling-broadened atomic' $\tilde{G}^r_{\sigma\sigma,0(U)}$ from equation (55). Analogous expressions for $B^0_{\alpha,\sigma}(\omega,t)$ and $B^U_{\alpha,\sigma}(\omega,t)$ can be obtained via the replacements $u_\alpha(t_1) \to u_\alpha(t_1)\,[1-n_{\bar\sigma}(t_1)]$ and $u_\alpha(t_1) \to u_\alpha(t_1)\,n_{\bar\sigma}(t_1)$, respectively.

Note that t enters (A.1) in two different ways: firstly, through the upper bound of the outer integral, and secondly since the exponential in the integrand depends explicitly on t. Therefore, evolving (A.1) from t to $t+\delta t$ yields

$$\begin{aligned} A^{0(U)}_{\alpha,\sigma}(\omega,t+\delta t) &= A^{0(U)}_{\alpha,\sigma}(\omega,t)\,\exp\left[\mathrm{i}\int_{t}^{t+\delta t} \mathrm{d}t_2\, F^{0(U)}_{\alpha,\sigma}(\omega,t_2)\right] \\ &\quad -\,\mathrm{i}\int_{t}^{t+\delta t} \mathrm{d}t_1\, u_\alpha(t_1)\,\exp\left[\mathrm{i}\int_{t_1}^{t+\delta t} \mathrm{d}t_2\, F^{0(U)}_{\alpha,\sigma}(\omega,t_2)\right]. \end{aligned} \tag{A.3}$$

Before the onset of time dependence, chosen without loss of generality at $t_0 = 0$, or in the stationary setup—cases both characterized by $\Delta(t) \equiv 0$ on the dot, $\Delta_\alpha(t) \equiv 0$ on the leads, and $\Gamma(t) \equiv \Gamma$—the integration may be performed analytically and yields

$$A^{0(U)}_{\alpha,\sigma}(\omega,0) = \frac{u_\alpha}{\omega - \varepsilon_{0(U)} - \mu_B B\sigma + \frac{\mathrm{i}}{2}\Gamma}\,, \tag{A.4a}$$

$$B^{0}_{\alpha,\sigma}(\omega,0) = \frac{u_\alpha\,[1-n_{\bar\sigma}(0)]}{\omega - \varepsilon_{0} - \mu_B B\sigma + \frac{\mathrm{i}}{2}\Gamma}\,, \text{ and} \tag{A.4b}$$

$$B^{U}_{\alpha,\sigma}(\omega,0) = \frac{u_\alpha\,n_{\bar\sigma}(0)}{\omega - \varepsilon_{0} - U - \mu_B B\sigma + \frac{\mathrm{i}}{2}\Gamma}\,. \tag{A.4c}$$

Equation (A.4*a*) suffice to determine the current and the dot occupancy in the stationary regime.

After the onset of time dependence, equation (A.3) will be used iteratively. For small enough time steps δt, both integrals may be evaluated approximately using the midpoint rule,

$$\begin{aligned} A^{0(U)}_{\alpha,\sigma}(\omega,t+\delta t) &= A^{0(U)}_{\alpha,\sigma}(\omega,t)\,\exp\left[\mathrm{i}\delta t\, F^{0(U)}_{\alpha,\sigma}(\omega,t_1)\right] \\ &\quad -\mathrm{i}\delta t\, u_\alpha(t_1)\,\exp\left[\frac{\mathrm{i}\delta t}{2}\, F^{0(U)}_{\alpha,\sigma}(\omega,t_2)\right] + \mathcal{O}(\delta t^3)\,, \end{aligned} \tag{A.5}$$

where $t_1 = t + \frac{1}{2}\delta t$ and $t_2 = t + \frac{3}{4}\delta t$ are the midpoints for the outer and inner integrals in equation (A.3). The corresponding expressions for $B^{0(U)}_{\alpha,\sigma}$ contain $n_{\bar\sigma}(t_1)$ which, if unknown, may be interpolated from the endpoints, i.e. $n_{\bar\sigma}(t_1) \simeq \frac{1}{2}\,[n_{\bar\sigma}(t) + n_{\bar\sigma}(t+\delta t)]$.

ORCID iDs

Dmitry V Anchishkin https://orcid.org/0000-0002-5685-9055
Roland Hayn https://orcid.org/0000-0002-7659-0073
Steffen Schäfer https://orcid.org/0000-0001-7681-4420

References

[1] Meirav U, Kastner M A and Wind S J 1990 *Phys. Rev. Lett.* **65** 771
[2] Kastner M A 1993 *Phys. Today* **46** 24
[3] Altshuler B L, Lee P A and Webb R A 1991 *Mesoscopic Phenomena in Solids* (*Modern Problems in Condensed Matter Sciences*) (Amsterdam: Elsevier)
[4] Ahoori R C 1996 *Nature* **379** 413
[5] Chorley S J, Galpin M R, Jayatilaka F W, Smith C G, Logan D E and Buitelaar M R 2012 *Phys. Rev. Lett.* **109** 156804
[6] Dyakov S A *et al* 2018 *Sci. Rep.* **8** 4911
[7] Quay C H L, Cumings J, Gamble S J, de Picciotto R, Kataura H and Goldhaber-Gordon D 2007 *Phys. Rev.* B **76** 245311
[8] Kastner M A 1992 *Rev. Mod. Phys.* **64** 849
[9] Goldhaber-Gordon D, Shtrikman H, Mahalu D, Abusch-Magder D, Meirav U and Kastner M A 1998 *Nature* **391** 156
[10] Costi T A and V Zlatić 2010 *Phys. Rev.* B **81** 235127
[11] Dubi Y and Di Ventra M 2011 *Rev. Mod. Phys.* **83** 131
[12] Azema J, Daré A-M, Schäfer S and Lombardo P 2012 *Phys. Rev.* B **86** 075303

[13] Whitney R S 2014 *Phys. Rev. Lett.* **112** 130601
[14] Daré A-M and Lombardo P 2017 *Phys. Rev.* B **96** 115414
[15] Le Hur K 2015 *Nature* **526** 203
[16] Iftikhar Z, Jezouin S, Anthore A, Gennser U, Parmentier F D, Cavanna A and Pierre F 2015 *Nature* **526** 233
[17] Keller A J, Peeters L, Moca C P, Weymann I, Mahalu D, Umansky V, Zaránd G and Goldhaber-Gordon D 2015 *Nature* **526** 237
[18] Hetsch F, Zhao N, Kershaw S V and Rogach A L 2013 *Mater. Today* **16** 312
[19] Xu J *et al* 2018 *Nat. Nanotechnol.* **13** 456
[20] Pathak S, Cao E, Davidson M C, Jin S and Silva G A 2006 *J. Neurosci.* **26** 1893
[21] Anderson P W 1961 *Phys. Rev.* **124** 41
[22] Keldysh L V 1964 *Zh. Eksp. Teor. Fiz.* **47** 1515
Keldysh L V 1965 *Sov. Phys.—JETP* **20** 1018
[23] Datta S 2005 *Quantum Transport: Atom to Transistor* (Cambridge: Cambridge University Press)
[24] Haug H and Jauho A 2010 *Quantum Kinetics in Transport and Optics of Semiconductors* (*Springer Series in Solid-State Sciences*) (Berlin: Springer)
[25] Jauho A-P, Wingreen N S and Meir Y 1994 *Phys. Rev.* B **50** 5528
[26] Smirnov S and Grifoni M 2013 *New J. Phys.* **15** 073047
[27] Stefanucci G and Kurth S 2018 *Phys. Rev.* B **97** 245415
[28] Croy A, Saalmann U, Hernández A R and Lewenkopf C H 2012 *Phys. Rev.* B **85** 035309
[29] Dong B, Ding G H and Lei X L 2015 *J. Phys.: Condens. Matter* **27** 205303
[30] Cohen G, Gull E, Reichman D R and Millis A J 2015 *Phys. Rev. Lett.* **115** 266802
[31] Anders F B and Schiller A 2005 *Phys. Rev. Lett.* **95** 196801
[32] Haldane F D M 1978 *Phys. Rev. Lett.* **40** 416
[33] Hewson A C 1993 *The Kondo Problem to Heavy Fermions* (Cambridge: Cambridge University Press)
[34] Hubbard J 1963 *Proc. R. Soc.* A **276** 238
[35] Hewson A C 1966 *Phys. Rev.* **144** 420
[36] Vovchenko V, Anchishkin D, Azema J, Lombardo P, Hayn R and Daré A-M 2014 *J. Phys.: Condens. Matter* **26** 015306
[37] Bickers N E, Cox D L and Wilkins J W 1987 *Phys. Rev.* B **36** 2036
[38] Myöhänen P, Stan A, Stefanucci G and van Leeuwen R 2009 *Phys. Rev.* B **80** 115107
[39] Eskes H, Meinders M B J and Sawatzky G A 1991 *Phys. Rev. Lett.* **67** 1035
[40] Lombardo P and Albinet G 2002 *Phys. Rev.* B **65** 115110
[41] Wingreen N S, Jacobsen K W and Wilkins J W 1989 *Phys. Rev.* B **40** 11834
[42] Langreth D C and Wilkins J W 1972 *Phys. Rev.* B **6** 3189
[43] Langreth D C 1976 Linear, nonlinear response theory with applications *Linear, Nonlinear Electron Transport in Solids* ed J T Devreese and V E van Doren (Boston, MA: Springer) pp 3–32
[44] Maciejko J 2007 *An Introduction to Nonequilibrium Many-Body Theory* (University Lecture) (http://www.physics.arizona.edu/~stafford/Courses/560A/nonequilibrium.pdf)
[45] Hofstetter W and Kehrein S 1999 *Phys. Rev.* B **59** R12732
[46] Schäfer S and Logan D E 2001 *Phys. Rev.* B **63** 045122
[47] Schäfer S 2011 *Phys. Rev.* B **83** 195110